Nuclear Instruments and Methods in Physics Research B 547 (2024) 165207

Contents lists available at ScienceDirect

Nuclear Inst. and Methods in Physics Research, B

journal homepage: www.elsevier.com/locate/nimb

Proton-beam energy diagnostics by color-center photoluminescence imaging in LiF crystals: Implementation of multiple Coulomb scattering into an analytical Bragg-curve model

E. Nichelatti [a,*], M. Piccinini [b], P. Nenzi [b], L. Picardi [b], C. Ronsivalle [b], R.M. Montereali [b]

[a] ENEA C.R. Casaccia, Fusion and Technology for Nuclear Safety and Security Dept., Via Anguillarese 301, Rome, Italy
[b] ENEA C.R. Frascati, Fusion and Technology for Nuclear Safety and Security Dept., Via E. Fermi 45, Frascati, Rome, Italy

ARTICLE INFO

Keywords:
Lithium fluoride
Color center
Proton beam
Photoluminescence
Bragg curve
Multiple Coulomb scattering

ABSTRACT

Lithium fluoride crystals are used to assess proton-beam energy spectra. Proton irradiation induces laser-active color centers in the crystal, whose density correlates with the absorbed dose. The spatial distribution of photoluminescence emitted by these color centers is exploited to estimate the proton-beam energy spectrum using an analytical Bragg-curve model. This study integrates the effects of multiple Coulomb scattering (MCS) into the model. At high enough energies, MCS leads to proton leakage through the crystal faces with a reduction in absorbed dose along the crystal length. The model incorporates MCS using an empirical approach based on Monte Carlo simulations.

1. Introduction

Radiation detectors based on photoluminescence (PL) from color centers (CCs) [1] in doped and undoped lithium fluoride (LiF) thin films and crystals have become a reliable choice in a wide range of applications, such as dosimetry [2–5], contact and phase-contrast X-ray imaging [6,7], ion track detection [8–11], and energy diagnostics of proton beams [12–22]. LiF plays a special role in the alkali halides family, due to its largest band gap (~14 eV) within all the solids [23], its hardness, its significant resistance to moisture, and light transparency from about 120 nm to 7 μm. Once exposed to ionizing radiation – gamma and X-rays, electrons, protons, α-particles, heavier ions – LiF hosts various electronic point defects, some of which are laser active and efficiently photoluminesce in the visible [24]. Among these, the most well-known are the F_2 and F_3^+ CCs, formed by two electrons bound to two and three anion vacancies, respectively, which are stable at room temperature (RT). They feature almost overlapping absorption bands at ~ 450 nm, which together form the so-called M band [25–28]. Under light excitation in this band, they show Stokes-shifted broad photoemission bands centered at 678 and 541 nm, respectively [26]. These spectral properties have been so far found to be independent of the incident ion beam species, energies, and fluencies.

Because of the high emission efficiencies and lasing characteristics [24], even at RT, of the F_2 and F_3^+ centers, many studies can be found in the literature regarding the optical properties of these point defects, produced in LiF crystals by means of several kinds of irradiation sources, and the complex behaviors related to transformations and interactions among different types of them. However, quantitative information for all the parameters that influence the relative concentrations of such active defects is not available in detail for LiF, although several practical recipes are available for a selective generation of the desired kind of defects and an improvement of the light emission performances.

One of the crucial problems concerning irradiated LiF is the coexistence of several kinds of aggregate defects with often overlapping absorption bands, which makes it difficult to clearly individuate and measure the actual contributions due to the individual centers in the optical absorption spectra. On the other hand, the intensities of PL spectra are relative to the measurement conditions, therefore there is still plenty of work to do for dosimetry based on PL from radiation-induced CCs in LiF. So far, on the basis of a number of systematic investigations conducted by our group, the visible PL response of LiF crystals and films irradiated with protons has been found to possess a linear behavior vs. dose below about 10^5-10^6 Gy [13,15,17,20,29,30].

As far as PL-imaging is concerned, it should be noted that the F_2 and F_3^+ CCs in LiF can serve as minimum luminescent units, enabling high intrinsic spatial resolution due to their atomic-scale dimensions,

* Corresponding author.
E-mail address: enrico.nichelatti@enea.it (E. Nichelatti).

https://doi.org/10.1016/j.nimb.2023.165207
Received 23 October 2023; Received in revised form 6 December 2023; Accepted 10 December 2023
Available online 14 December 2023

typically comparable to the lattice spacing. Remarkably, a spatial resolution of 80 nm was achieved in soft X-ray micro-radiographs stored in LiF thin films and examined using scanning near-field optical microscopy [31].

Regarding the use of PL-based LiF radiation detectors for energy diagnostics of proton beams, in the past years our group has been routinely characterizing the energy spectrum of the output beam of the TOP-IMPLART proton linear accelerator (linac) – under assembly and testing in the C.R. Frascati research labs of ENEA in the framework of the TOP-IMPLART project (Oncological Therapy with Protons-Intensity Modulation Proton Linear Accelerator for Radiotherapy) [32,33] – during the stages of its modular development [15,17–19,21,22,33]. A unique feature of such accelerators is the ability to adjust beam intensity and energy on a pulse-by-pulse basis. Beam dynamics calculations demonstrate that the methods employed for this purpose – setting the energy by deactivating specific accelerating modules while adjusting the power in the last active module, and controlling intensity by varying either the source injected charge or the duration of the radiofrequency (RF) pulse – not only influence the final energy of the beam, but also shape its energy spectrum. Characterizing the energy spectrum of the beam is therefore crucial for verifying the correct operation of the linac. Our group achieves this goal by acquiring in a fluorescence microscope the two-dimensional PL-intensity map generated in typically 1-mm thick LiF crystals by CCs induced by proton beam irradiation at grazing incidence. From this map, a luminescent replica of the Bragg curve is suitably extracted, provided the irradiation dose is not too high to cause saturation of the CCs density [15,20,29]. This PL-intensity profile along the depth is then fitted using an analytical model for proton Bragg curves in LiF [18] or directly inverted by applying an iterative algorithm [19].

Multiple Coulomb scattering (MCS) [34] is a phenomenon that occurs when charged particles, such as protons, traverse a material. Specifically, when a proton traverses the LiF crystal lattice, its trajectory can be deflected due to multiple collisions with the nuclei and electrons. This scattering is caused by the electrical interaction between the proton and the particles in LiF. Since LiF is composed of lithium and fluorine atoms, which have positive and negative electrical charges, respectively, protons will be influenced by the Coulombic forces generated by these charges. MCS is a random process and results in an angular distribution of particles that pass through the material.

The effect of MCS on the deposition of dose by protons and consequent distribution of CCs in LiF thin films was already analyzed at 35 MeV [22] and in the range 1–8 MeV [35] by using Monte Carlo (MC) simulations conducted in FLUKA [36–39]. In this paper, we implement the effect of MCS in the analytical model for Bragg curve formation in LiF crystals under grazing incidence of the beam. MCS causes proton leakage from the crystal faces, leading to a gradual decrease in the depth-fluence curve and a modification of the linear energy transfer (LET) depth curve, especially at higher proton energies. To characterize proton beam energies beyond our previous scope, we introduce this depth-LET curve modification into the analytical Bragg curve model using an empirical approach based on FLUKA simulations. Practical applications of this method are demonstrated.

2. Materials and methods

The TOP-IMPLART linac comprises a series of linear accelerating modules added sequentially, generating a proton beam pulse with a duration of about 3 μs at a repetition rate of 25 Hz. These modules are grouped into sections, each powered by a 10 MW peak power klystron. Currently, the linac is in development phase and consists of eight modules, delivering a nominal proton beam output of 71 MeV.

In the second example of Section 6, a commercially available (Mateck GmbH, Germany) $15 \times 10\ mm^2$ and 1 mm-thick LiF crystal with both sides polished was used.

The fluorescence microscope used to acquire the PL-intensity map of the LiF crystal reported in the second example of Section 6 is a Nikon Eclipse 80i equipped with a Hg lamp, a 4 × objective and an Andor NEO camera.

The LINAC software [40] was used for beam dynamics simulations giving the energy spectrum of Fig. 4(a).

The Bragg-curve analytical model used to fit the simulated dose and experimental PL-intensity depth profiles is coded in MATLAB 7.10 [41], including the implementation of the MCS effects described in Sections 4 and 5. All the MC simulations reported in this work were performed with the particle-transport software FLUKA 4–3.3 [36–38] and its graphical interface Flair 3.2–4.5 [39] on a 12th Gen Intel(R) Core(TM) i9-12900 K, 3.20 GHz workstation equipped with 64 GB Ram. The elaborations of the MC simulations used to determine the parameters of the MCS correction of the Bragg-curve model were done in Wolfram Mathematica 13.3 [42].

3. Proton beam energy diagnostics with photoluminescent color centers in LiF crystals

The experimental setup employed for assessing the energy spectrum of the linac proton beam involves placing a LiF crystal along the beam propagation path. The beam, assumed to be collimated, transversally wide, and homogeneous over an area larger than the typical crystal thickness, impacts the crystal in air at ideally perfect grazing incidence (grazing angle = 0°). Specifically, the thinnest face of the LiF crystal, typically 1-mm thick in our experiments, is oriented perpendicular to the incoming protons, causing them to propagate within the crystal along its longer dimension and generate CCs in it. Certain CCs in LiF, such as the F_2 and F_3^+ aggregates, are laser active and emit Stokes-shifted broad-band visible PL in the red and green spectral ranges, respectively, upon blue light excitation [25–28]. In a second step, the irradiated crystal is observed from its top face using a fluorescence microscope to acquire a two-dimensional map of PL. The intensity of this map, attributed to contributions from CCs homogeneously created throughout the entire crystal thickness, is assumed to be directly proportional to the absorbed dose within the crystal, provided that the dose does not reach levels high enough to cause density saturation [29]. This enables the extraction of a PL-intensity profile versus penetration depth, which can be fitted using an appropriate model. As this profile shape and depth, in addition to the material density and molar mass, are related to the proton beam energy spectrum, an assessment of the latter can be derived from the fitting outcome. The actual occurrence of a 0° grazing angle incidence of the beam can be confirmed by observing the gradual decrease to zero of the PL-intensity profile at penetration depths greater than the Bragg-peak depth. If this condition is not met, it is likely that a slight misalignment of the crystal occurred during the mounting procedure, resulting in protons from inclined trajectories in air irradiating the crystal either from its top or bottom face.

It is worth noting that the crystal thickness of 1 mm is selected as a compromise. Indeed, using thinner crystals would result in a lower detectable PL intensity due to the emission from a smaller volume of CCs, leading to a poorer signal-to-noise ratio. This is particularly important for potential characterizations at clinical doses for radiotherapy. Conversely, acquiring the PL from CCs formed by irradiation in a thicker crystal with a fluorescence microscope would yield a blurred PL-intensity map. This is because the microscope objective would capture contributions from both in-focus and out-of-focus planes along the crystal thickness. After conducting various tests, we concluded that a 1 mm thickness represents an optimal compromise for our intended purposes.

As far as the choice of LiF is concerned, it was chosen due to our team's extensive experience with this material and with the formation in it of visible-luminescent CCs upon exposure to protons and various forms of ionizing radiation. The linearity between PL intensity and absorbed dose [29], as well as dose-rate independence of its response [30], assist in (a) analyzing the luminescent Bragg curves detected and measured in LiF crystals for proton-beam energy diagnostics, and (b)

correlating the simulated absorbed dose with the concentration of formed color centers. In principle, other materials exhibiting similar luminescent properties could serve the purpose of proton Bragg-curve detection and storing. For instance, F_2^+ centers in CaF_2 also emit visible light, peaking around 660 nm under optical excitation at 360 and 570 nm [43]. However, proper tests and measurements should be conducted with this material to assess its sensitivity and suitability for recording proton Bragg curves with good response linearity.

In the past years, the model we have been routinely using to fit the experimentally obtained PL-intensity depth profiles is based on an analytical approximation of the proton Bragg curve in LiF [18], which extends Bortfeld's theory for proton Bragg curves in water [44]. In our previous analyses, the finite thickness of the LiF crystal used as radiation detector was not considered. This is because, for the involved proton energies (up to ~ 30 MeV), we assumed that the crystal thickness would not sensibly affect the distribution of absorbed dose within the crystal and, consequently, the detected PL map used for extracting the PL-intensity depth profile. However, for proton energies high enough to cause a non-negligible fraction of beam protons to leak from the crystal faces, these dimensions can no longer be ignored. It is worth noting that the assumption of the proton beam being collimated, transversally wide, and homogeneous over an area larger than the crystal thickness is a common configuration in our experimental setup. This configuration enables the approach presented in this paper. Addressing different scenarios would likely necessitate a comprehensive treatment with Monte Carlo simulations.

The primary reason for proton leakage from the crystal faces is MCS. When a proton enters the LiF detector, it experiences multiple collisions with the ions of the crystal lattice. Each collision introduces a slight deviation in the proton trajectory, with the scattering angle being related to the atomic number, density, and electron density of the material. In cases where the initial proton energy is sufficiently high, and numerous scattering events accumulate as the particle travels through the crystal, the proton can be laterally displaced by an amount large enough to cross one of the crystal faces and exit in air. A schematic representation of this fact is depicted in Fig. 1. As a result, the proton continues its path in the air, no longer contributing to energy deposition in the LiF crystal, unless scattering events in air, much less probable due to the low density of this medium, occur and redirect the particle towards the crystal.

An example illustrating the significant impact of MCS is presented in Fig. 2. This example, simulated with FLUKA, considers 100 MeV protons entering a 1-mm thick LiF crystal at 0° grazing incidence and compares it with an ideally bulk LiF detector. In the case of the bulk detector, the decrease in fluence along the penetration depth (z axis) is primarily attributed to the effect of inelastic nuclear interactions. However, for the 1-mm thick crystal, this effect combines with proton leakage caused by MCS, resulting in a dramatic reduction of both fluence and linear energy transfer (LET) towards the proton range.

Fig. 3 provides another example of the significant effects of MCS. This figure presents plots showing the percentage of protons that initially entered the LiF crystal and subsequently leaked into the air through its faces. The data represent a range of thicknesses from 0.5 to 2.5 mm and proton energies from 12 to 100 MeV. These results were also calculated using FLUKA simulations.

In the following Section, we demonstrate how we incorporate the effect of proton leakage, along with the resulting depth-LET curve modification, into the analytical model for the proton Bragg curve in LiF.

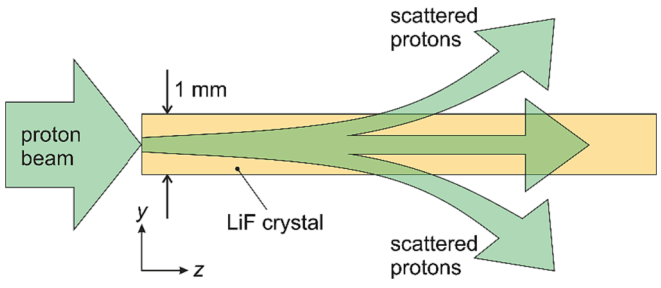

Fig. 1. Schematic representation of proton leakage through the LiF crystal faces due to multiple scattering events along the proton trajectories inside the crystal.

4. Theory

With the purpose of developing a fully analytical model for MCS-modified Bragg curves in LiF, in our first attempt we considered using a formula for pencil-beam fluence, which expands as the pencil beam propagates in a material [45]. Our plan was to describe any collimated proton beam as a continuous superposition of laterally shifted pencil beams, obtaining in this way an expression for the fluence inside a finite-thickness LiF crystal of a transversally wide proton beam. While mathematically feasible, this approach did not reproduce the results of test MC simulations we performed in FLUKA to verify its correctness. We ascribe this to the fact that the pencil-beam fluence formula is not usable when the border between LiF and air lies within the pencil-beam width.

Because we needed a practical way to analyze measured PL-intensity depth profiles and characterize the energy of the TOP-IMPLART beam, we decided to abandon the fully analytical approach and implement the effects of proton leakage using an empirical method. To achieve this, we simulated a series of depth-LET curves $L_{cr}(E,h;z)$ – with E, h and z being the proton energy, the crystal thickness and the propagation depth, respectively – in a LiF crystal using FLUKA, considering crystal thicknesses ranging from 0.5 to 2.5 mm and proton energies from 18 to 100 MeV, for a total of 50 simulations. In the simulations, the proton beam was impinging on the crystal at 0° grazing incidence, perpendicularly to the thinnest face of the crystal. Note that using FLUKA for this task ensures that a lot of physical processes – such as ionization, elastic and anelastic scattering, nuclear and electromagnetic interactions, radioactive decays, etc. – are properly taken into account [36–38]. The simulated depth-LET curves were compared to corresponding ones, $L_B(E;z)$, calculated using our analytical Bragg curve model for protons in bulk LiF [18]. For each couple of such curves, we calculated the ratio curve $r(E,h;z) = L_{cr}(E,h;z)/L_B(E;z)$ and fitted it in Mathematica with the function $\exp(-at^b)$ – where t represents the depth z normalized to the proton range R – which proved satisfactory for all the proton energies and crystal thicknesses. In this way, we obtained values of the a and b fit parameters for each (E,h) couple. The obtained values of a and b were in turn fitted, again in Mathematica, using the functions

$$a(E,h) = a_0\frac{E^{a_1}}{h^{a_2}}, \qquad b(h) = b_0\left(1 - e^{-b_1 h}\right), \tag{1}$$

$a_\alpha(\alpha = 0, 1, 2)$ and b_β $(\beta = 0, 1)$ being new fit parameters. For b, dependence on E was found to be not significant. These fitting functions are plotted, together with the a and b data, in Fig. 4. The obtained values of the fit parameters are listed in Table 1. together with their uncertainties evaluated at 95 %-confidence level. Note that the chosen expressions for $a(E,h)$ and $b(h)$ ensure that $r(E,h;z) = \exp\left[-a(E,h)(z/R)^{b(h)}\right] \to 1$ as $h \to \infty$. This is, indeed, a desired behavior, because a bulk can be seen as a crystal of infinite thickness.

Using the above results, we implement the effect of proton leakage due to MCS by multiplying the analytical expression of the Bragg curve for protons in LiF bulk by the ratio function $r(E,h;z)$. The result of this multiplication is assumed to be a practical formula for calculating the depth-LET curve within a LiF crystal of thickness h for protons of energy E impinging at 0° grazing incidence. Multiple test comparisons with FLUKA simulations were conducted to validate this assumption, with successful results.

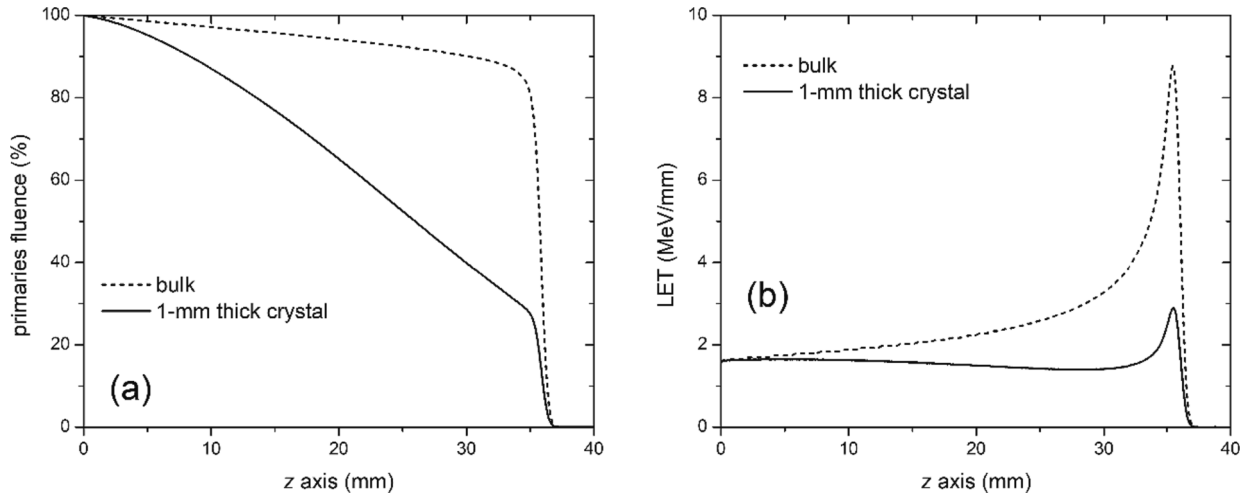

Fig. 2. FLUKA-simulated effects of MCS on (a) fluence and (b) depth-LET curves inside a 1-mm thick LiF crystal irradiated at 0° grazing incidence with a 100 MeV proton beam (solid lines), compared to their counterparts in LiF bulk (dashed lines).

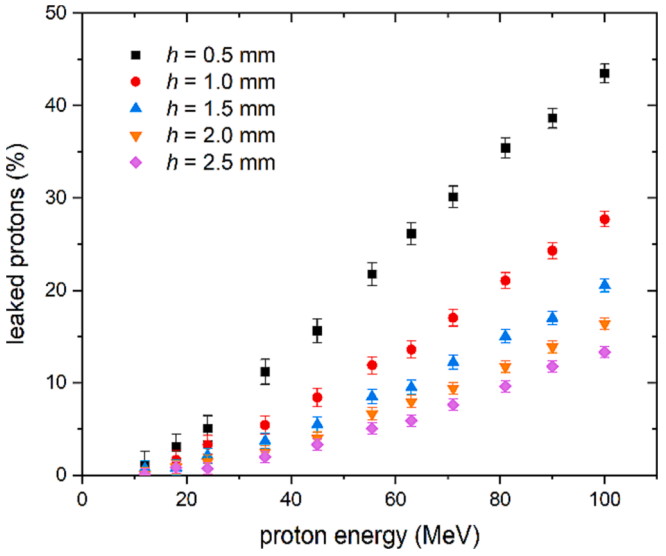

Fig. 3. Percentages of protons that initially entered the LiF crystal and subsequently leaked into the air through its faces. Data calculated from FLUKA simulations for representative values of crystal thickness and proton energy.

5. Discussion

As previously mentioned, once the depth-LET curve in LiF bulk has been calculated analytically, we can approximate the corresponding curve in a crystal of thickness h, irradiated at 0° grazing incidence by a wide and homogeneous proton beam of energy E, with

$$L_{cr}(E,h;z) = r(E,h;z)L_B(E;z). \tag{2}$$

Using the previously discussed analytical representation of $r(E,h;z)$, whose parameters have been obtained through best fits as demonstrated in Section 4, to derive an analytical representation of $L_{cr}(E,h;z)$ with Eq. (2) is significantly more efficient in terms of computational speed compared to adopting a look-up-table approach. In the latter method, $L_{cr}(E,h;z)$ would be calculated for each value of E and h by suitably interpolating the depth-LET curves resulting from the available FLUKA simulations.

If the proton beam is not monochromatic, assuming linearity of the cumulative energy deposition of protons with distinct energies and indicating the energy spectrum with $S(E)$, the depth-LET curve in the crystal can be written as

$$\mathscr{L}(h;z) = \int_0^{+\infty} S(E)r(E,h;z)L_B(E;z)\mathrm{d}E. \tag{3}$$

In the following examples, we employ Eq. (3) to estimate the energy spectrum of proton beams irradiating LiF crystals at 0° grazing incidence

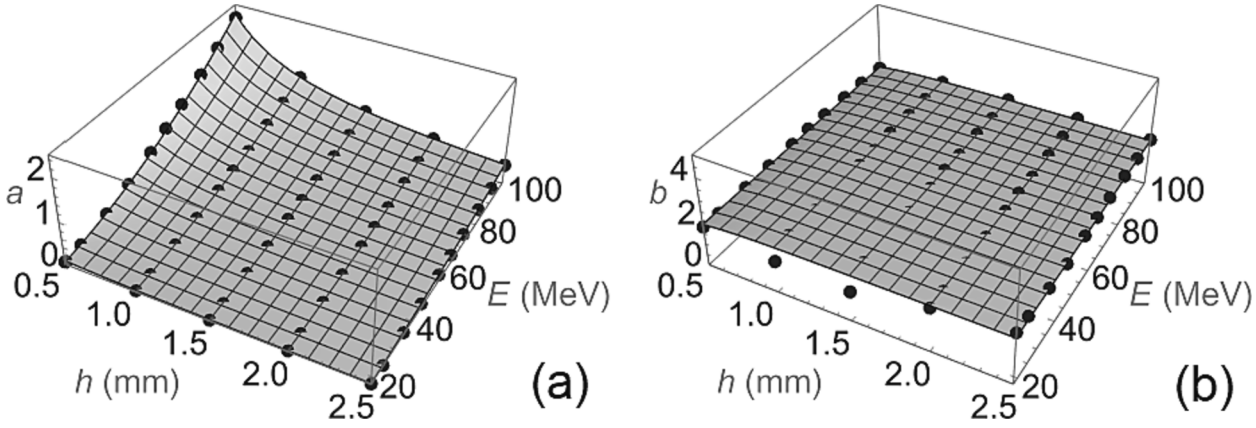

Fig. 4. Distributions of the data (black points) obtained for parameters (a) a and (b) b vs. proton energy E and crystal thickness h, along with the corresponding best-fitting surfaces (in gray), $a(E,h)$ and $b(h)$ – see Eq. (1) – whose parameters are reported in Table I.

Table 1
Best-fitting values of the parameters in $a(E,h)$ and $b(h)$.

$a_0(10^{-4}\mathrm{mm}^{a_2}/\mathrm{MeV}^{a_1})$	a_1	a_2	b_0	$b_1(\mathrm{mm}^{-1})$
1.90 ± 0.15	1.891 ± 0.019	0.9761 ± 0.0087	2.114 ± 0.013	4.76 ± 0.19

by fitting a suitably normalized $\mathscr{L}(h;z)$ to dose and PL-intensity depth profiles. While for the bulk case such a task was accomplished by representing the energy spectrum as a linear combination of Gaussian distributed energy components [18], in the present study we adopt an alternative approach. This approach is based on representing $S(E)$ with a histogram, where each bin has a height that corresponds to the spectral density of the energy interval covered by the bin width. In the fitting process, the number of bins can be set and changed according to the desired energy sampling, while their heights are optimized using a random optimization (also known as localized random search [46]) algorithm. The spectrum uncertainties are subsequently estimated with a 95 %-confidence level using the bootstrap method [47].

6. Examples

To validate our MCS-modified model within the optimization process for assessing the energy spectrum of a transversally wide, homogeneous proton beam irradiating a finite-thickness LiF crystal at 0° grazing incidence, we examine two example cases: a simulated percentage depth-dose (PDD) curve and an experimental PL-intensity depth profile.

6.1. Simulated 71 MeV proton irradiation of a LiF crystal

In the current development stage of the TOP-IMPLART proton linear accelerator, a 360° phase shifter is employed to adjust the phase of the accelerating field within the final two modules. While an essentially monochromatic output energy of 71 MeV is anticipated when the phase is set to 0°, non-zero values of the phase are expected to result in broader and more complex energy spectra. We simulated one of such spectra with a phase value of 45° using the LINAC software. The spectrum is reported in Fig. 5(a) as a light-gray histogram with bin widths chosen according to Scott's rule [48]. The same figure reports the median spectrum (black solid line) with 95 %-confidence uncertainties (represented by dark-gray bands) estimated by fitting the PDD curve shown in Fig. 5(b). This latter curve (gray thick solid line), shown together with its best fit (black solid line), was generated by using the energy spectrum obtained by the LINAC software as input in FLUKA to simulate proton irradiation at 0° grazing incidence on a 1-mm thick LiF crystal.

6.2. Experimental 45 MeV proton irradiation of a LiF crystal

During an early commissioning of the TOP-IMPLART linac with only six modules installed, a 1-mm thick LiF crystal was irradiated at 0° grazing incidence with a proton beam of nominal energy 55.5 MeV in a beam delivery setup used for *in vitro* radiobiology experiments. The dose at the LiF entry face was 30 Gy and the dose rate was 2 Gy/min. Before reaching the crystal, the beam propagated through a 50-μm thick Ti window, 0.5 mm of Al, a 600-μm thick Pb diffuser, 2 m of air, and the 1.5-mm thick polystyrene wall of the cell culture flask. According to estimations based on SRIM software [49], the passage through those media reduced the beam energy to approximately 45 MeV. The diameter of the central part of the beam that could be considered homogeneous at the LiF crystal position was about 2 cm.

While our analysis, whose results are shown in Fig. 6, confirmed the 45 MeV energy value, it also revealed a lower-energy component of about 18 MeV, corresponding to the passage of a 35 MeV component through the above-mentioned sequence of media. We ascribe the presence of this secondary component to faults of a klystron for a fraction of the total pulses.

Fig. 6(a) shows the experimental PL-intensity depth profile (gray thick solid line) extracted from the PL image map due to the CCs formed in the LiF crystal, together with its best-fitting profile (black solid line) obtained by applying our analysis. The corresponding energy spectrum estimated in this way is reported in Fig. 6(b). It features two peaks at the above-mentioned energies of 45 and 18 MeV.

To validate the obtained result, the energy spectrum of Fig. 6(b) was used as the input energy distribution in a FLUKA simulation. In order to replicate the experimental setup, the simulation consisted of irradiating a 1-mm thick LiF at 0° grazing incidence with a transversally wide and homogeneous proton beam. As shown in Fig. 7, the obtained depth-LET curve was suitably normalized to compare it with the experimental PL-intensity depth profile. The good replication of this latter confirms that our analysis has been accurate. Out of curiosity, Fig. 7 shows also how the simulated PL-intensity depth profile would be in LiF bulk, that is, if the finite thickness of the LiF crystal was not considered.

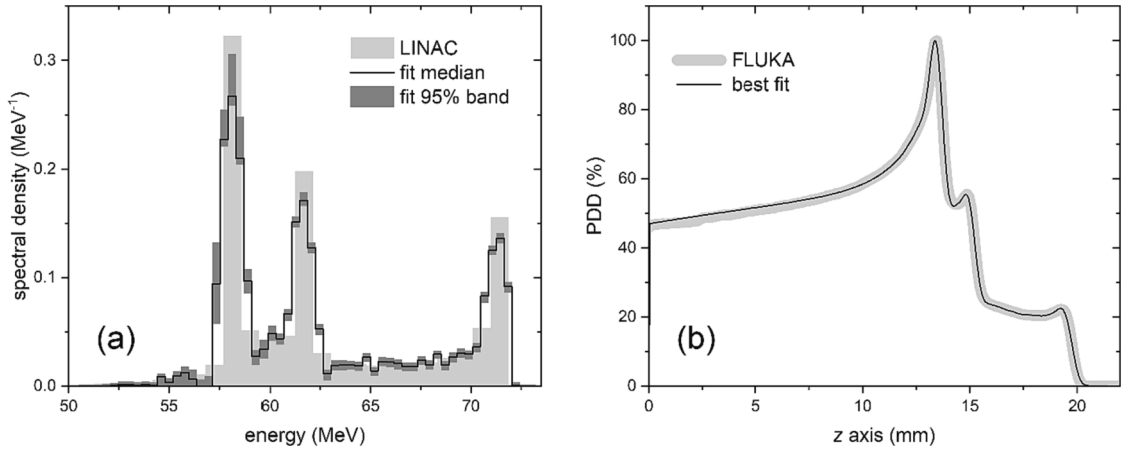

Fig. 5. (a) Proton-beam energy spectra generated by the LINAC software (light gray) and obtained by the best fit process (black solid line). The 95%-confidence bands of this latter are plotted in dark gray. (b) PDD curve in a 1-mm thick LiF crystal as simulated at 0° grazing incidence by FLUKA (gray thick solid line) using the LINAC energy spectrum shown in (a), and its best fit (black solid line).

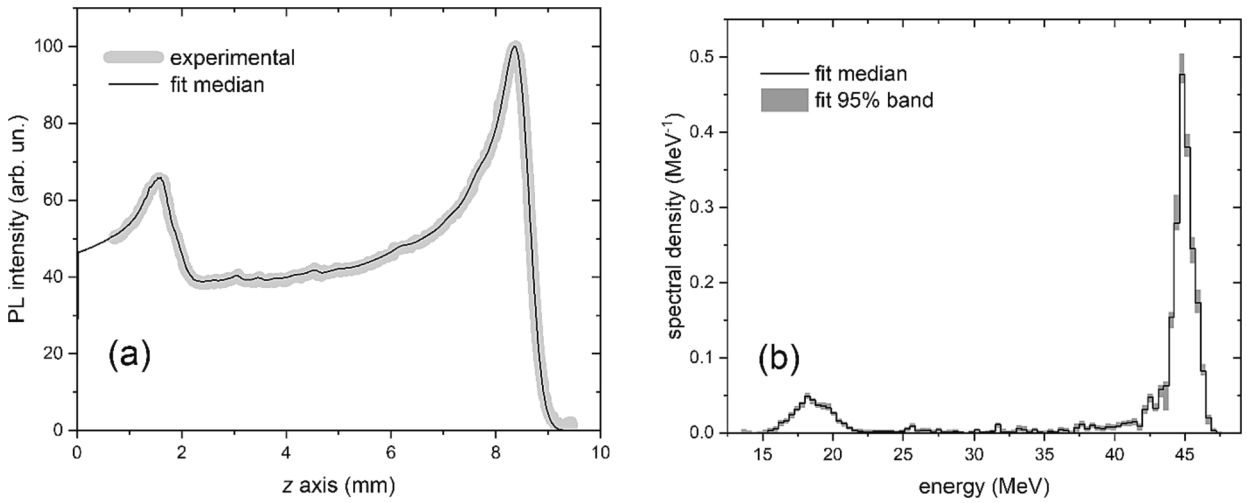

Fig. 6. (a) Experimental PL-intensity depth profile (gray thick solid line) measured in a 1-mm thick LiF crystal irradiated at 0° grazing incidence by a nominally 55.5 MeV proton beam, and its best fit (black solid line). (b) Proton-beam energy spectrum (black solid line) resulting from the fitting process, shown with its 95 %-confidence uncertainties (dark-gray bands).

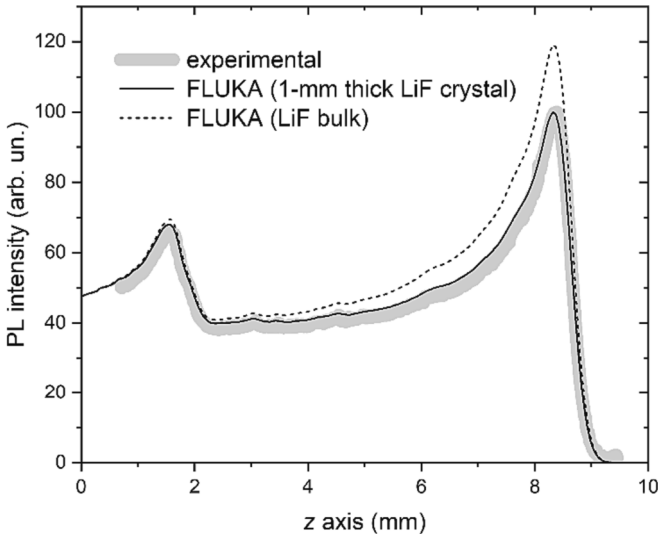

Fig. 7. Experimental PL-intensity depth profile (gray thick solid line) measured in a 1-mm thick LiF crystal irradiated at 0° grazing incidence by a nominally 55.5 MeV proton beam transmitted through different media, alongside the corresponding normalized depth-LET curve (black solid line) simulated by FLUKA under the same irradiation conditions using the energy spectrum from Fig. 5(b). The depth-LET curve that would be obtained with FLUKA under the same conditions for a LiF bulk, instead of a 1-mm thick LiF crystal, is also depicted (dashed line).

7. Conclusions and outlook

The analyses we have conducted so far of simulated dose and experimental PL-intensity depth profiles of radiation-induced CCs in LiF crystals have proved successful under double-check validations with FLUKA simulations using the obtained energy spectra. Two representative examples of such outcomes are those reported in Section 6. Regarding the energy spectra, in this paper for the first time we have represented them as histograms and employed a random optimization algorithm for their estimation, while in past studies we represented the spectra with linear combinations of Gaussian components. We believe that, thanks to the possibility of setting the desired energy sampling by using a proper number of bins, the method shown here can be more useful to deal with irregular spectra where Gaussian components cannot be clearly identified.

An alternative to the method presented in this paper could involve 3D-modelling the PL intensity due to proton irradiation of a thick enough LiF crystal. Despite the significantly increased complexity involved in handling a 3D model, detecting a 3D PL-intensity distribution would necessitate the use of confocal microscopy, contrasting with the simpler approach using fluorescence microscopy in 2D. Furthermore, FLUKA simulations suggest that at a standard clinical energy of 100 MeV, proton leakage could be considered negligible (i.e., leaked fluence below 1 %, for illustration purposes) for a crystal entry face thicker than ~ 7.5 mm (assuming a uniformly transverse proton beam). Such a thickness would result in a significantly increased cost of good optical-quality and polished LiF crystals, although the technologies are available. Additionally, employing a confocal fluorescence microscope would require prolonged acquisition times. Therefore, while a 3D approach might theoretically offer an interesting alternative worth investigating, the associated complexity and costs may not necessarily streamline procedures compared to considering proton leakage within our simpler model.

The proposed method will be further applied in future energy characterizations of the TOP-IMPLART beam as additional modules are integrated into the linac to increase the output energy. Additionally, our ongoing efforts will focus on addressing experimental PL-intensity depth profiles stored by CCs in LiF crystals that were not perfectly aligned with the proton beam.

Declaration of competing interest

The authors declare that they have no known competing financial interests or personal relationships that could have appeared to influence the work reported in this paper.

Acknowledgments

Many thanks are due to A. Ampollini for his skillful technical assistance. The authors are also indebted with many colleagues, researchers, technicians, students, and guests contributing to the TOP-IMPLART project. This research has been carried on within the TOP-IMPLART (Oncological Therapy with Protons – Intensity Modulated Proton Linear Accelerator for Radiotherapy) project, funded by Regione Lazio, Italy, and the TECHEA (Technologies for Health) project, funded by the Italian National Agency for New Technologies, Energy and Sustainable Economic Development (ENEA), Italy.

Statement.

During the preparation of this work the authors used OpenAI ChatGPT 3.5 in order to only review and enhance certain English grammar and sentence structures. After using this service, the authors reviewed and edited the content as needed and take full responsibility for the content of the publication.

References

[1] W.B. Fowler, Physics of Color Centers, Academic Press, New York, 1968.
[2] W.L. McLaughlin, Colour Centres in LiF for Measurement of Absorbed Doses up to 100 MGy, Radiat. Prot. Dosimetry 66 (1996) 197–200.
[3] W.L. McLaughlin, J.M. Puhl, A. Kovács, M. Baranyai, I. Slezsák, M.C. Saylor, S. A. Saylor, S.D. Miller, M. Murphy, Sunna dosimeter: an integrating photoluminescent film and reader system; work in progress, Radiat. Phys. Chem. 55 (1999) 767–771.
[4] J.E. Villarreal-Barajas, M. Piccinini, M.A. Vincenti, F. Bonfigli, R.F. Khan, R. M. Montereali, Visible photoluminescence of color centers in LiF crystals for absorbed dose evaluation in clinical dosimetry, IOP Conf. Ser.: Mater. Sci. Eng. 80 (2015), 012020.
[5] M. Piccinini, E. Nichelatti, M. Pimpinella, V. De Coste, R.M. Montereali, Dose response of visible color center radiophotoluminescence in lithium fluoride crystals irradiated with a reference ^{60}Co gamma beam in the 1–20 Gy dose range, Radiat. Meas. 151 (2022), 106705.
[6] G. Baldacchini, F. Bonfigli, F. Flora, R.M. Montereali, D. Murra, E. Nichelatti, A. Faenov, T. Pikuz, High-contrast photoluminescent patterns in lithium fluoride crystals produced by soft x-rays from a laser-plasma source, Appl. Phys. Lett. 80 (2002) 4810.
[7] G. Baldacchini, F. Bonfigli, A. Faenov, F. Flora, R.M. Montereali, A. Pace, T. Pikuz, L. Reale, Lithium Fluoride as a Novel X-ray Image Detector for Biological μ-World Capture, J. Nanosci. Nanotechno. 3 (2003) 483.
[8] P. Bilski, B. Marczewska, Fluorescent detection of single tracks of alpha particles using lithium fluoride crystals, Nucl. Instrum. Methods Phys. Res. B 392 (2017) 41–45.
[9] P. Bilski, B. Marczewska, W. Gieszczyk, M. Kłosowski, T. Nowak, M. Naruszewicz, Lithium fluoride crystals as fluorescent nuclear track detectors, Radiat. Prot. Dosim. 178 (2018) 337–340.
[10] P. Bilski, B. Marczewska, W. Gieszczyk, M. Kłosowski, M. Naruszewicz, M. Sankowska, S. Kodaira, Fluorescent imaging of heavy charged particle tracks with LiF single crystals, J. Lumin. 213 (2019) 82–87.
[11] M. Sankowska, P. Bilski, B. Marczewska, Thermal enhancement of the intensity of fluorescent nuclear tracks in lithium fluoride crystals, Radiat. Meas. 157 (2022), 106845.
[12] M. Piccinini, F. Ambrosini, A. Ampollini, M. Carpanese, L. Picardi, C. Ronsivalle, F. Bonfigli, S. Libera, M.A. Vincenti, R.M. Montereali, Solid state detectors based on point defects in lithium fluoride for advanced proton beam diagnostics, J. Lumin. 156 (2014) 170–174.
[13] M. Piccinini, F. Ambrosini, A. Ampollini, L. Picardi, C. Ronsivalle, F. Bonfigli, S. Libera, E. Nichelatti, M.A. Vincenti, R.M. Montereali, Photoluminescence of radiation-induced color centers in lithium fluoride thin films for advanced diagnostics of proton beams, Appl. Phys. Lett. 106 (2015), 261108.
[14] M. Piccinini, C. Ronsivalle, A. Ampollini, G. Bazzano, L. Picardi, P. Nenzi, E. Trinca, M. Vadrucci, F. Bonfigli, E. Nichelatti, M.A. Vincenti, R.M. Montereali, Proton beam spatial distribution and Bragg peak imaging by photoluminescence of color centers in lithium fluoride crystals at the TOP-IMPLART linear accelerator, Nucl. Instrum. Methods Phys. Res. A 872 (2017) 41–51.
[15] E. Nichelatti, M. Piccinini, A. Ampollini, L. Picardi, C. Ronsivalle, F. Bonfigli, M. A. Vincenti, R.M. Montereali, Bragg-curve imaging of 7 MeV protons in a lithium fluoride crystal by fluorescence microscopy of colour centres, EPL 120 (2017) 56003.
[16] B. Marczewska, P. Bilski, T. Nowak, W. Gieszczyk, M. Kłosowski, Imaging of proton Bragg peaks in LiF, Radiat. Prot. Dosim. 178 (2018) 333–336.
[17] M. Piccinini, E. Nichelatti, C. Ronsivalle, A. Ampollini, G. Bazzano, F. Bonfigli, P. Nenzi, V. Surrenti, E. Trinca, M. Vadrucci, M.A. Vincenti, L. Picardi, R. M. Montereali, Visible photoluminescence of color centers in LiF crystals for advanced diagnostics of 18 and 27 MeV proton beams, Radiat. Meas. 124 (2019) 59–62.
[18] E. Nichelatti, C. Ronsivalle, M. Piccinini, L. Picardi, R.M. Montereali, An analytical approximation of proton Bragg curves in lithium fluoride for beam energy distribution analysis, Nucl. Instrum. Methods Phys. Res. B 446 (2019) 29–36.
[19] E. Nichelatti, C. Ronsivalle, M. Piccinini, L. Picardi, R.M. Montereali, Algorithm for inversion of photoluminescent Bragg curves in lithium fluoride applied to the analysis of proton beam energy spectra, Nucl. Instrum. Methods Phys. Res. B 459 (2019) 36–42.
[20] R.M. Montereali, M. Piccinini, A. Ampollini, L. Picardi, C. Ronsivalle, F. Bonfigli, E. Nichelatti, M.A. Vincenti, Visible photoluminescence of color centers in lithium fluoride detectors for low-energy proton beam Bragg curve imaging and dose mapping, Opt. Mater. 95 (2019), 109242.
[21] M. Piccinini, E. Nichelatti, A. Ampollini, G. Bazzano, C. De Angelis, S. Della Monaca, P. Nenzi, L. Picardi, C. Ronsivalle, V. Surrenti, E. Trinca, M. Vadrucci, M. A. Vincenti, R.M. Montereali, Dose response and Bragg curve reconstruction by radiophotoluminescence of color centers in lithium fluoride crystals irradiated with 35 MeV proton beams from 0.5 to 50 Gy, Radiat. Meas. 133 (2020), 106275.
[22] E. Nichelatti, V. Nigro, M. Piccinini, M.A. Vincenti, A. Ampollini, L. Picardi, C. Ronsivalle, R.M. Montereali, Photoluminescent Bragg curves in lithium fluoride thin films on silicon substrates irradiated with a 35 MeV proton beam, J. Appl. Phys. 132 (2022), 014501.
[23] M. Piacentini, A new interpretation of the fundamental exciton region in LiF, Solid State Commun. 17 (1975) 697–700.
[24] T.T. Basiev, S.B. Mirov, V.V. Osiko, Room-temperature color center lasers, IEEE J. Quantum Electron. 24 (1988) 1052–1069.
[25] J. Nahum, D.A. Wiegand, Optical Properties of Some F-Aggregate Centers in LiF, Phys. Rev. 154 (1967) 817–830.
[26] G. Baldacchini, M. Cremona, R.M. Montereali, U.M. Grassano, V. Kalinov, *Emission properties of irradiated LiF crystals excited in the F absorption band by an excimer laser*, in "Defects in Insulating Materials", Vol. 2 (O. Kanert and J. M. Spaeth, Eds.), pp. 1103-1105, World Scientific, Singapore, 1993.
[27] G. Baldacchini, M. Cremona, G. d'Auria, R.M. Montereali, V. Kalinov, Radiative and Nonradiative Processes in the Optical Cycle of the F3+ Center in LiF, Phys. Rev. B 54 (1996) 17508–17514.
[28] G. Baldacchini, E. De Nicola, R.M. Montereali, A. Scacco, V. Kalinov, Optical bands of F2 and F3+ centers in LiF, J. Phys. Chem. Solids 61 (2000) 21.
[29] E. Nichelatti, M. Piccinini, A. Ampollini, L. Picardi, C. Ronsivalle, F. Bonfigli, M. A. Vincenti, R.M. Montereali, Modelling of photoluminescence from F2 and F3+ colour centres in lithium fluoride irradiated at high doses by low-energy proton beams, Opt. Mater. 89 (2019) 414–418.
[30] M. Piccinini, E. Nichelatti, M.A. Vincenti, V. Nigro, C. Ronsivalle, A. Ampollini, P. Nenzi, G. Bazzano, E. Trinca, R.M. Montereali, Dynamic range and dose linearity of the radioluminescence intensity in lithium fluoride crystals irradiated with 2.3 and 26 MeV protons, J. Lumin. 259 (2023), 119833.
[31] A. Ustione, A. Cricenti, F. Bonfigli, F. Flora, A. Lai, T. Marolo, R.M. Montereali, G. Baldacchini, A. Faenov, T. Pikuz, L. Reale, Micro-Radiographs Stored in Lithium Fluoride Films Observed by Scanning Near-Field Optical Microscopy, Jpn. J. Appl. Phys. 45 (2006) 2116–2118.
[32] C. Ronsivalle, M. Carpanese, C. Marino, G. Messina, L. Picardi, S. Sandri, E. Basile, B. Caccia, D.M. Castelluccio, E. Cisbani, S. Frullani, F. Ghio, V. Macellari, M. Benassi, M. D'Andrea, L. Strigari, The TOP-IMPLART Project, Eur. Phys. J. plus 126 (2011) 68.
[33] L. Picardi, A. Ampollini, G. Bazzano, E. Cisbani, F. Ghio, R.M. Montereali, P. Nenzi, M. Piccinini, C. Ronsivalle, F. Santavenere, V. Surrenti, E. Trinca, M. Vadrucci, E., Wembe Tafo, *Beam commissioning of the 35 MeV section in an intensity modulated proton linear accelerator for proton therapy*, Phys. Rev. Accel. Beams 23 (2020), 020102.
[34] B. Gottschalk, in: *Physics of Proton Interactions in Matter*, in "proton Therapy Physics", CRC Press, Boca Raton, 2011, pp. 19–60.
[35] R.M. Montereali, V. Nigro, M. Piccinini, M.A. Vincenti, A. Ampollini, P. Nenzi, C. Ronsivalle, E. Nichelatti, Bragg Curve Detection of Low-Energy Protons by Radiophotoluminescence Imaging in Lithium Fluoride Thin Films, Sensors 23 (2023) 4779.
[36] The official CERN FLUKA website. Available online: https://fluka.cern (Accessed on 4 October 2023).
[37] G. Battistoni, T. Boehlen, F. Cerutti, P.W. Chin, L.S. Esposito, A. Fassò, A. Ferrari, A. Lechner, A. Empl, A. Mairani, A. Mereghetti, P. Garcia Ortega, J. Ranft, S. Roesler, P.R. Sala, V. Vlachoudis, G. Smirnov, Overview of the FLUKA code, Ann. Nucl. Energy 82 (2015) 10–18.
[38] C. Ahdida, D. Bozzato, D. Calzolari, F. Cerutti, N. Charitonidis, A. Cimmino, A. Coronetti, G.L. D'Alessandro, A. Donadon Servelle, L.S. Esposito, R. Froeschl, R. García Alía, A. Gerbershagen, S. Gilardoni, D. Horváth, G. Hugo, A. Infantino, V. Kouskoura, A. Lechner, B. Lefebvre, G. Lerner, M. Magistris, A. Manousos, G. Moryc, F. Ogallar Ruiz, F. Pozzi, D. Prelipcean, S. Roesler, R. Rossi, M. Sabaté Gilarte, F. Salvat Pujol, P. Schoofs, V. Stránský, C. Theis, A. Tsinganis, R. Versaci, V. Vlachoudis, A. Waets, M. Widorski, New Capabilities of the FLUKA Multi-Purpose Code, Front. Phys. 9 (2022), 788253.
[39] V. Vlachoudis, FLAIR: *A Powerful But User Friendly Graphical Interface For FLUKA*, in Proc. Int. Conf. on Mathematics, Computational Methods & Reactor Physics (M&C 2009), Saratoga Springs, New York, 2009.
[40] K.R. Crandall, M. Weiss, TERA 94/34 ACC 20 internal note (1994).
[41] MATLAB, v. 7.10.0 (R2010a), The MathWorks Inc., Natick, Massachusetts, 2010. Website URL: http://www.mathworks.com.
[42] Mathematica, v. 13.3, Wolfram Research Inc., Champaign, Illinois, 2023. Website URL: https://www.wolfram.com/mathematica.
[43] T. Kato, D. Nakauchi, N. Kawaguchi, T. Yanagida, Radio-photoluminescence properties of CaF_2 transparent and opaque ceramics, Curr. Appl. Phys. 20 (2020) 1195–1200.
[44] T. Bortfeld, An analytical approximation of the Bragg curve for therapeutic proton beams, Med. Phys. 24 (1997) 2024–2033.
[45] B. Gottschalk, On the scattering power of radiotherapy protons, Med. Phys. 37 (2010) 352–367.
[46] J.C. Spall, in: *Stochastic Optimization*, in "handbook of Computational Statistics", Springer, Berlin, 2004, pp. 169–197.
[47] M. Bonamente, Statistics and Analysis of Scientific Data, 2nd ed., Springer, New York, 2017, pp. 230–234.
[48] D.W. Scott, On optimal and data-based histograms, Biometrika 66 (1979) 605–610.
[49] J.F. Ziegler, M.D. Ziegler, J.P. Biersack, SRIM – The stopping and range of ions in matter 2010, Nucl. Instrum. Methods Phys. Res. B 268 (2010) 1818–1823.